1985

Turbulence Measurements with a submarine

Osborn, Thomas R.; Lueck, Rolf G.

Osborn, Thomas R., and Rolf G. Lueck. "Turbulence measurements with a submarine." Journal of physical oceanography 15.11 (1985): 1502-1520.
http://hdl.handle.net/10945/62197

Turbulence Measurements with a Submarine

THOMAS R. OSBORN* AND ROLF G. LUECK

Department of Oceanography, Naval Postgraduate School, Monterey, CA 93943

(Manuscript received 19 March 1984, in final form 29 May 1985)

ABSTRACT

Measurements of small-scale velocity and temperature fluctuations have been made from the research submarine *Dolphin* in the open ocean off San Diego, California. The important contribution of the submarine is that it collects horizontal profiles. The submarine can depth-cycle to obtain a quasi-vertical profile of the fluctuations along a horizontal path. The noise level depends on the configuration of the instrumentation and the operating conditions of the vessel. Expressed in terms of energy dissipation, it is approximately 10^{-7} W m^{-3}, comparable to that of free-fall vertical profilers.

Much of the small-scale velocity and temperature data are similar to those collected with free-fall vertical profilers. A major difference is that the horizontal transects are aligned with the temperature gradient of salt fingers, which are not well detected by vertical profilers. Fingers were seen beneath the saline upper layer at values of $R\rho$ between 2 and 4. Off San Diego, the velocity signal from the fingers was below the noise level of the velocity probes.

More than 80% of our estimates of the local rate of dissipation of kinetic energy from a nighttime convecting surface layer are distributed log-normally. There is a deficit of large values and an excess of small values, as in atmospheric boundary layers.

1. Introduction

Measurements of the small-scale velocity and temperature fluctuations in the upper ocean were obtained from the research submarine *Dolphin* over the continental shelf off San Diego, California in December 1980 and April 1982. Section 2 describes the instrumentation and the operational characteristics of the submarine as they affect turbulence measurements. Data shown in Section 3 demonstrate the unique capabilities of the system. The distribution of a large data set from a convecting upper layer is examined in Section 4. The appendix details the errors of the dissipation estimates.

The pioneering oceanic turbulence measurements by Grant *et al.* (1962) were horizontal measurements from a towed body in a tidal channel. Mounting their probes on a submarine operating in the open Pacific Ocean (Grant *et al.*, 1968), they found sharp interfaces separating turbulent regions from quiet layers. The sharp vertical intermittency and the vertical displacement due to internal waves produced a complex combination of isopycnal and diapycnal variation. This work inspired the measurement of vertical profiles of microstructure that originally focused on temperature fluctuation measurements (Osborn and Cox, 1972). Later, techniques for small-scale salinity and density measurements were developed (Gregg *et al.*, 1973). Finally, velocity fluctuations (Osborn, 1974) were measured from vertically profiling instruments.

The body developed by Grant *et al.* was used through the 1960s and into the 1970s in both coastal waters and the open Pacific (Nasmyth, 1970; Gargett, 1975, 1976). In the early 1970s, a Pisces submersible was outfitted for measurements of ocean turbulence (Gargett, 1982). The hot-film velocity sensor from the towed body was augmented with airfoil probes, and, for the first time, all three components of the turbulent velocity fluctuations were measured simultaneously. The success of that work enabled access to the *Dolphin* for turbulence measurements. The *Dolphin* is a true submarine, not a submersible, capable of extended operations in open water without a surface vessel for support.

2. Instrumentation

The *Dolphin* is a diesel-electric submarine owned and operated by the U.S. Navy. Specifically designed for research, it is 51 m (165 feet) long and 5.6 m (18 feet) in diameter. The hull is cylindrical with a hemispherical bow. The front of the pressure hull is not the bow of the ship. There is a false bow of steel plate over a framework of steel scaffolding that forms a free-flooding chamber, which is pumped dry for installation of transducers, wires, and miscellaneous fittings.

In order to put the probes in relatively undisturbed flow with minimal contamination by false velocity signals from vibration of the structure, they are mounted

* Present affiliation: Chesapeake Bay Institute, Shady Side, MD. 20764.

4.92 m (16 feet) above the hull of the submarine atop a tower (Figs. 1 and 2). The three main legs of the frame are 0.25 m diameter thick-wall steel pipe, capped at both ends and pressurized with dry nitrogen. The pipes are sealed to reduce their effective masses and increase their natural frequencies of vibration.

The sensors are located above the bow rather than along the axis of the submarine for several reasons: 1) The present location is much less expensive for initial installation and for work on the electronics and probes. No divers are required to change probes or electronics, 2) The flow distortion is no worse at this location than at an equivalent distance in front of the bow, which is a stagnation point, 3) The mounting points for the frame are much stronger in their present location (attached directly to the pressure hull rather than the false bow), 4) The probes are out of the water during transit, docking and battery charging, and 5) We can profile through the very surface of the ocean with the probes mounted above the hull.

The instrumentation consists of three separate systems: a ship status system, an acoustic current meter and CTD package, and a turbulence package. The ship status system, integral with the vessel, measures the ship's functions (heading, pitch, roll, shaft rpm, etc.).

Water column and ship speed data are collected by a Neil Brown Instrument Systems CTD and an acoustic current meter system supplied by the Applied Physics Laboratory of the Johns Hopkins University. The CTD includes the normal NBIS 0.03 m conductivity cell, a platinum thermometer, and a fast-response thermistor. The acoustic current meter has a three-component head. The main pressure case for the NBIS electronics is located near the front leg of the frame. A velocity head with 0.2 m path lengths is mounted on the front of this pressure case. For the early tests in 1980 the CTD sensor was mounted along the shaft supporting the velocity head. In April 1982 another velocity head (with 0.1 m spacing) and the conductivity and temperature sensors were mounted near the top of the tripod 0.56 m below the turbulence package. Figure 2 shows the sensors in April 1982.

FIG. 1. The USS *Dolphin* (AGSS 555) with instrumentation mounted for the April 1982 measurements. Transducers for the turbulent velocity and temperature fluctuations are atop the tripod.

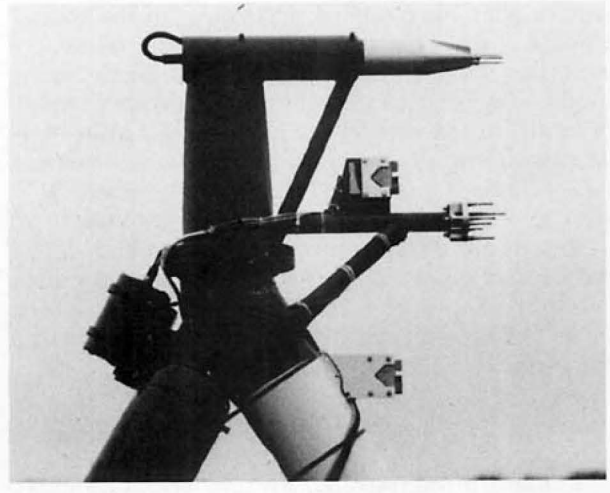

FIG. 2. Detailed view of the turbulence package and upper acoustic current meter transducers for the April 1982 measurements.

The turbulence instrumentation measures two perpendicular components of the turbulent velocity fluctuations with airfoil probes (Osborn and Crawford, 1980). One probe is aligned to sense vertical velocity fluctuations w, and the other is aligned for horizontal velocity fluctuations v, perpendicular to the direction of travel. The temperature and its gradient are measured with a fast thermistor (Thermometrics FP07). The gradient is derived by analog processing. Three orthogonal accelerometers are mounted 0.72 m aft of the airfoil probes. Pressure and its rate of change are measured by a pressure transducer and associated circuit mounted in the bow.

More details on the instrumentation are given by Osborn and Lueck (1985a) and Osborn *et al.* (1981). A detailed comparison of the acoustic current meter and the foil probes for scales between 10 m and 0.1 m is presented by Osborn and Lueck (1984).

3. Data

a. Operations

The *Dolphin* has been used for three sets of cruises. The first, in October 1980, tested the frame and turbulence instrumentation. A spectrum analyzer and chart recorder recorded the data. For the second cruise, in December 1980, the NBIS instrumentation and digital recording of the turbulence data were added. On the third cruise, April 1982, hydrographic (CTD and XBT) and turbulence (Camel II) profiles were simultaneously made from the R. V. *Acania.*

On each dive the submarine follows a predetermined

pattern which is modified depending on the characteristics of the water column. The submarine can operate in a "level flight" mode or in a depth-cycling mode. The latter can be either: 1) slow ascents and descents, with a vertical excursion of 100 m or more and a wavelength of several kilometers, or 2) more rapid cycles through a limited depth range of about 30 m with a wavelength on the order of one kilometer.

Results are shown from two dives; the first was on the night of 4 December 1980 and the second was on 22 April 1982. Both dives were 20 km offshore from La Jolla, California, and consist of a transect from near the surface to 100 m depth.

b. 4 December 1980 data

In Fig. 3 the salinity, density and temperature data are shown as vertical profiles although they were collected over a large horizontal distance. Initially the vessel was heading north at approximately 1 m s^{-1}. After 3.6 km the vessel turned and went back 1.5 km. There is a mixed layer extending to about 35 db below which the temperature generally decreases with a broad salinity minimum between 40 and 80 db. The forward speed varied from 0.8 to 1.3 m s^{-1}, with a brief burst of speed to 1.8 m s^{-1}.

From the pressure signal we know the data start just below 30 db with the submarine descending slowly to 36 db, rising to 15 db and then descending to 65 db. The submarine then rises, sinks, rises again, and finally descends to 100 db. The vertical speed is always less than 0.03 m s^{-1}. This up-and-down fluctuation of the vessel is associated with ballast and trim of the vessel as well as control problems at low operating speed. The submarine is difficult to control since it has no sailplanes or bowplanes, just tailplanes. The increase in density with depth requires that the submarine take on water to descend. During this profile, water was brought into the ballast tank twice, first to get through the thermocline and again at about 60 m depth when the vessel started to "float" up. In spite of a real spirit of cooperation from the crew, it is not possible to make the vessel go up or down at a moment's notice. It is often necessary to adjust the ballast and the trim (pitch angle) before the submarine responds properly.

Three minutes of turbulence data at 63 m depth are shown (Fig. 4) with sufficient bandwidth to display all the variance of the signal. The velocity shear data are displayed twice, once with a 20 Hz low-pass filter to show the turbulent fluctuations and again with no filter to show the high-frequency noise. The speed of the vessel at this time was 0.95 m s^{-1}. Spectra of the three components of acceleration (Fig. 5) were calculated from eight blocks of 4096 points. The data were first differenced, their average removed, a cosine taper applied to the ends, transformed, and the transformed values recolored. The spectral estimates were then averaged over eight adjacent frequency bands and over eight contiguous blocks. The digitization rate was 500 Hz so the final spectral resolution is close to 1 Hz. The smallest accelerations are in the vertical direction while the largest are in the lateral direction with major peaks at 30 and 40 Hz which do not appear in the other components. The frame is weakest in the lateral direction because the separation of the back legs is limited by the beam of the vessel and the curvature of the hull. There are also peaks in the accelerometer spectra between 55 and 70 Hz. Beyond these frequencies, the spectra roll off owing to the characteristics of the electronics.

The right-hand scaling (Fig. 5) is an estimate of the velocity shear contamination due to vibration of the velocity probes assuming 1) that the acceleration is the same at the velocity probes and at the accelerometers (not satisfied since the velocity probes and the accelerometers are separated by 0.72 m in the axial direc-

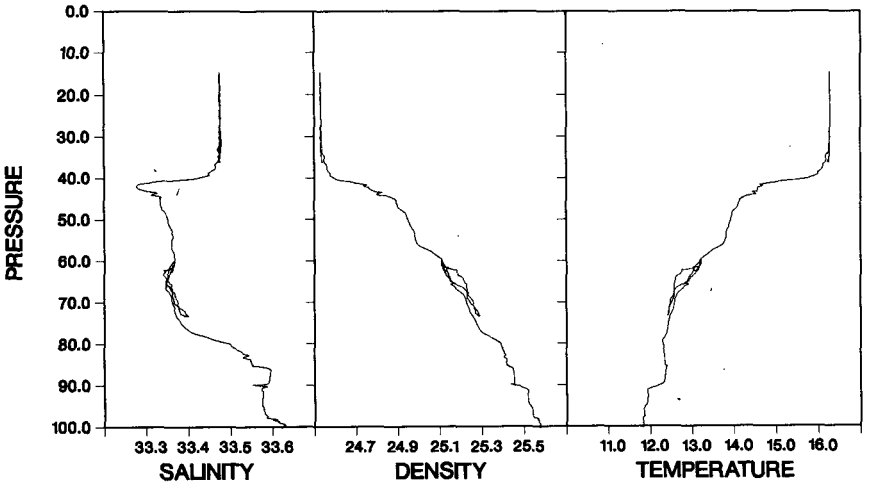

FIG. 3. Salinity, density and temperature profiles from 4 December 1980.

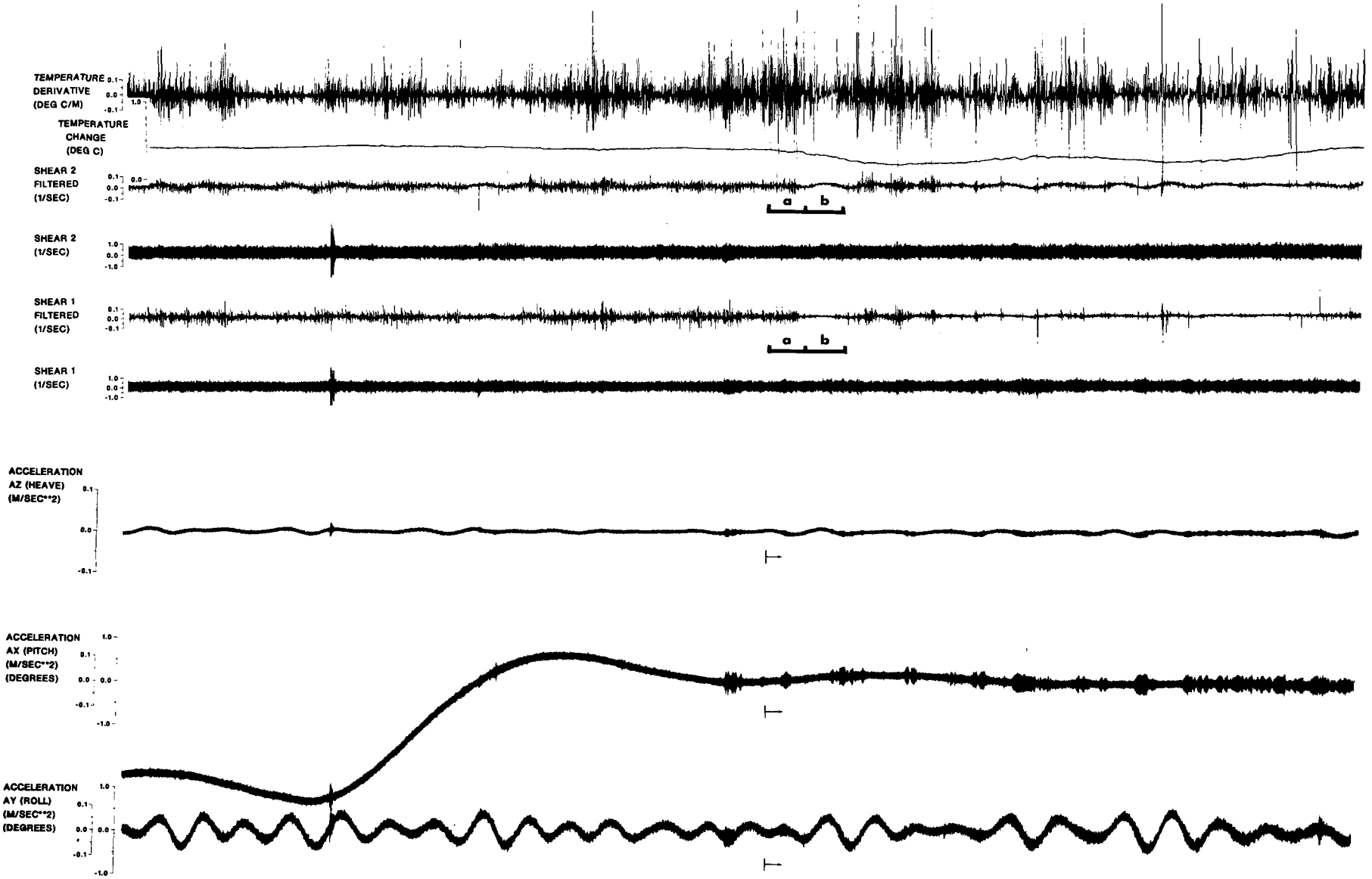

FIG. 4. A sample of the turbulence data from a depth of 63 m on 4 December 1980. The filtered shear channels have been low-pass filtered at 20 Hz to show the turbulent fluctuations while the unfiltered channels show all the variance. Shear is $\partial w/\partial x$.

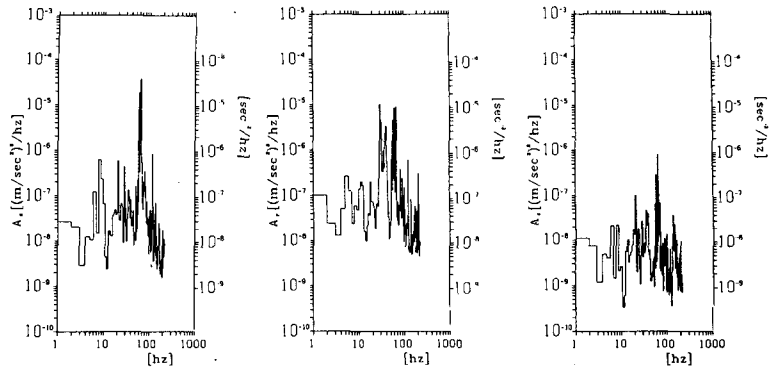

FIG. 5. Spectra of the accelerometer data shown in Fig. 4. The axes on the left are in terms of acceleration; the axes on the right are in terms of velocity shear. The data begin at the arrows below the accelerometer traces in Fig. 4.

tion), and 2) that the probes have no inherent acceleration sensitivity (laboratory measurements show none). The estimated contamination is a^2/U^2 (Moum and Lueck, 1985).

Velocity shear spectra (Figs. 6 and 7) from active (a) and quiet (b) regions (Fig. 4) have similar shapes above 40 Hz but differ in the low-frequency region. This low-frequency region is the dissipation spectrum. The data labeled (b) (Fig. 4) are from a relatively quiet region where the dissipation estimated from the variance of the shear using the isotropic formula:

$$\epsilon = 7.5\rho\nu[\langle(\partial w/\partial x)^2\rangle + \langle(\partial v/\partial x)^2\rangle]/2, \quad (1)$$

is 3×10^{-7} W m^{-3}. In region (a) the dissipation estimate is 16 times greater, 5×10^{-6} W m^{-3}.

The noise level of the velocity shear spectra in the data band is well above the level of the vibrational contamination. This situation is markedly different from our measurements with a towed body (Osborn and Lueck, 1985b) where the velocity-scaled accelerometer spectral levels are within a factor of 2 of the levels of the velocity shear from 1 to 50 Hz. The ac-

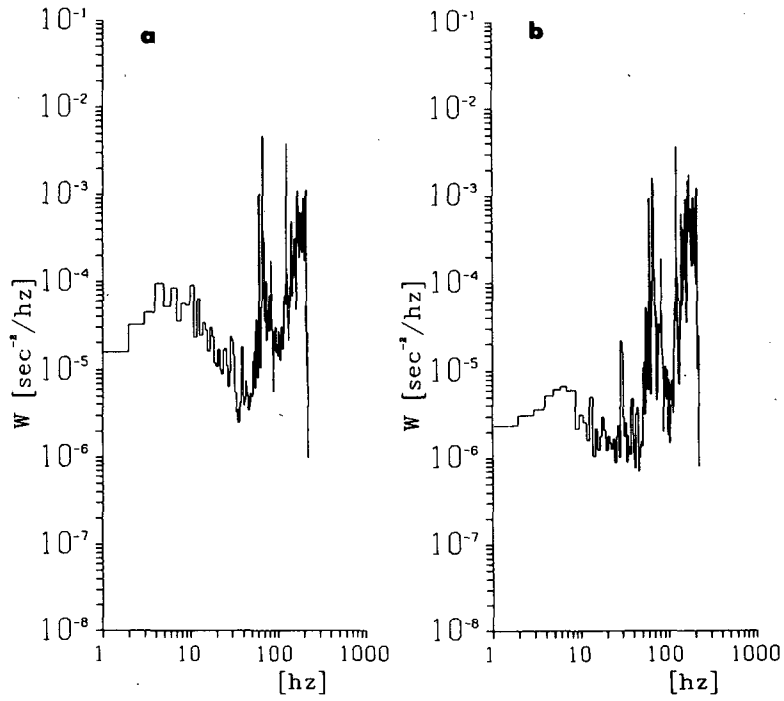

FIG. 6. Spectra of the downstream fluctuations of the vertical velocity for the $\partial w/\partial x$ data in Fig. 4. The variation of the low-frequency portion of the spectrum is due to variations in the intensity of the turbulent fluctuations. The spectra are calculated from 4096 points representing 8 s in time marked "a" and "b" in Fig. 4.

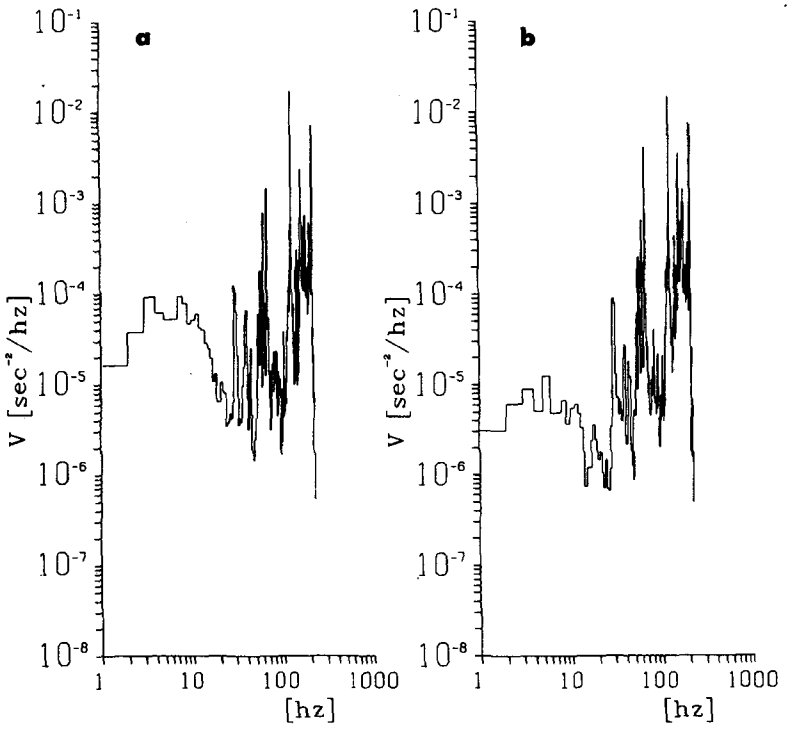

FIG. 7. Spectra of the downstream variations of the lateral horizontal velocity fluctuations ($\partial v/\partial x$) for the data shown in Fig. 4.

celerometers are 0.3 m from the shear probes on the towed body electronics package, 60% closer. That may explain part of the difference in the two results. Another difference is that the top piece of the submarine frame can flex about the mounting flange just aft of the upper acoustic current meter head (Fig. 2). Since that location is directly below the accelerometers the motion is axial at the accelerometers but has a vertical component at the location of the airfoil probes.

To calculate estimates of the dissipation rate for the entire dataset, noise spikes due to plankton hitting the probe were removed and replaced by a linear interpolation over the interval. Spectra were computed in blocks of 4096 points and examined in conjunction with the chart records. The variance was integrated to 20, 35, or 50 Hz depending on the value of the integral to 10 Hz. The variance estimates from both probes were combined with speed and viscosity (Miyake and Koizumi, 1948) using the isotropic relationship and plotted (Fig. 8).

In December 1980 we did not collect surface observations of atmospheric and oceanographic conditions; the Fleet Numerical archives indicate surface cooling and evaporation. Figure 8 shows an active surface mixing layer where the individual estimates of dissipation vary by a factor of 10. Near the bottom of the mixing layer and above the depth of maximum temperature gradient, the rate of dissiption is significantly less than in the bulk of the mixing layer. The fluctuations in the mean temperature profile indicate entrainment of water into the upper layer. Dissipation increases again in the top of the thermocline (where the temperature gradient has a maximum) before dropping sharply by a factor of 1000. The drop-off occurs at a temperature 1°C lower than that in the mixing layer. The vertical displacement between dissipation values can be estimated from the pressure derivative. At the base of the mixed layer, where the dissipation decreases dramatically, the rate of descent is 0.012 m s^{-1}; so the vertical extent of each estimate is 0.1 m and the horizontal extent is 6.6 m. Data from this upper layer are examined further in the discussion (Section 4).

Near 63 db, large dissipation values were observed during one of the three times that we sampled that depth interval. At that same depth but in different locations, the dissipation values were as much as 1000 times smaller. For the profile as a whole, the largest dissipation values are at 63 db depth and the next largest values are in the thermocline at about 45 db depth. The lowest levels, below 10^{-7} W m^{-3}, represent the noise floor of the system.

While lower speeds (0.8–1.3 m s^{-1}) allow the submarine to cover more distance before surfacing to charge the batteries, sometimes it is necessary to operate at higher speeds. When surfacing, speed is used to force the vessel to the surface quickly. Submariners do not like to be in the depth range where the periscope is submerged so that they cannot see through it, yet they

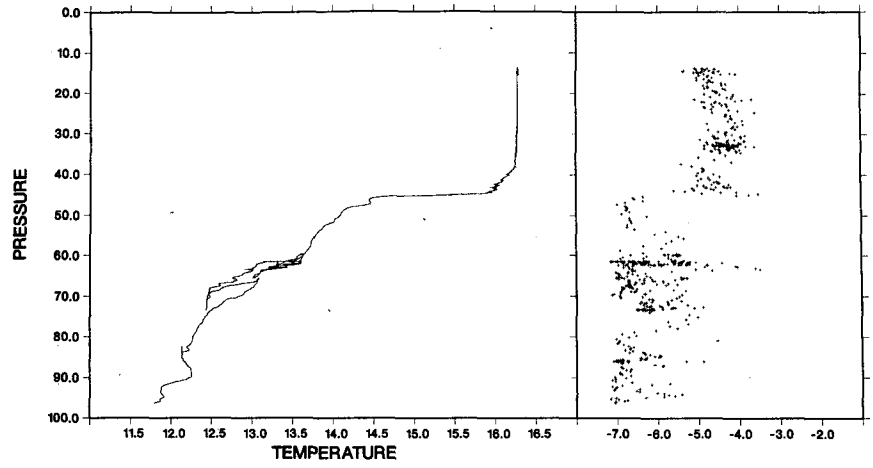

FIG. 8. The calculated dissipation rate for the 4 December 1980 profile of the *Dolphin*. The dissipation rate is plotted on a logarithmic scale in units of W m^{-3}. The value represents the average of the estimates from the vertical and the horizontal velocity shear data over 8-second intervals.

are not below keel depth of surface vessels. At 1.8 m s^{-1} there is substantially more signal in the accelerometer channels, (Fig. 9) with a larger vibrational peak in all three components just below 20 Hz (Fig. 10), than at lower speeds (Figs. 4 and 5). When scaled by the speed squared, to estimate contamination to the shear measurements, the spectra are comparable to the lower-speed spectra in terms of amplitude as a function of frequency.

The 20 Hz vibration in the velocity shear spectra (Figs. 11 and 12) is substantially higher than the accelerometer spectra predict. The peak in $\partial w/\partial x$ can be explained as rotation about the flange (no explanation is available for the peak in $\partial v/\partial x$). If the noise level of the system is represented by Fig. 11a and Fig. 12a for the two channels, then the noise when integrated to, but not including, the vibrational peak is 3×10^{-7} W m^{-3}. The situation is not as satisfactory as at the lower speed, for at higher speeds there is a vibrational peak right in the dissipation region. Fortunately, that vibrational peak is exceded by the real signal at a dissipation rate 10 times the noise level.

c. *April 1982*

The mean temperature, salinity, and density fields from the dive on 22 April 1982 (Fig. 13) were taken on a transect from the surface downward, along a northerly heading. The profiles are similar to the 1980 profiles except that the upper layer is thermally stratified and the salinity minimum is not so thick.

The second acoustic current meter head and the NBIS conductivity and temperature sensors were placed at the apex of the tripod. This addition of mass near the top of the frame produced vibrational spikes at 18, 22, and 25 Hz which cause no serious problem for the measurements of dissipation (Fig. 14). The temperature profile from the CTD fast thermistor is used because of noise contamination of the temperature data from the turbulence package. Temperature gradient data from the turbulence package are unaffected by the noise. The turbulence and CTD sensors are 0.56 m apart vertically. For a transect that is plotted as a profile, it is appropriate to remove the offset in depth between the temperature and dissipation profiles. So, while the temperature and dissipation values come from the same pressure, they represent different horizontal locations. The dissipation profile is substantially different from that in December 1980. There is no surface-forced turbulent layer. There are intermittent patches of turbulence, e.g., the 4 m thick relatively mixed layer centered at 15 db. The noise level is 2×10^{-7} W m^{-3} based on an integral from 1 to 13 Hz. As before, the integral extends to progressively higher frequencies as the dissipation rate increases.

The CTD data from 22 April 1982 (Fig. 13) show a salinity minimum, with warmer water above, so salt fingering is possible (Turner, 1973). The *T–S* plot shows that both temperature and salinity decrease with depth from 35 (14.25°C) to 41 db (13°C). Examination of the temperature gradient-data shows several patches (Fig. 15, labeled A–E) that we interpret as salt fingers because 1) the signal is amplitude-limited, 2) the spectra are band-limited, and 3) a velocity shear signal is absent. There are turbulent patches containing both temperature-gradient and velocity shear fluctuations near the beginning and end of the data in Fig. 15a. The irregular and spiky nature of the temperature gradient in these patches contrasts sharply with the features labeled A–E, which appear more uniform in amplitude. Gargett and Schmitt (1982) show similar time series. Spectra (Fig. 16) show the difference between the first turbulent patch in Fig. 15a and the salt fingers labeled A. There is a deficit of variance in the salt fingers at

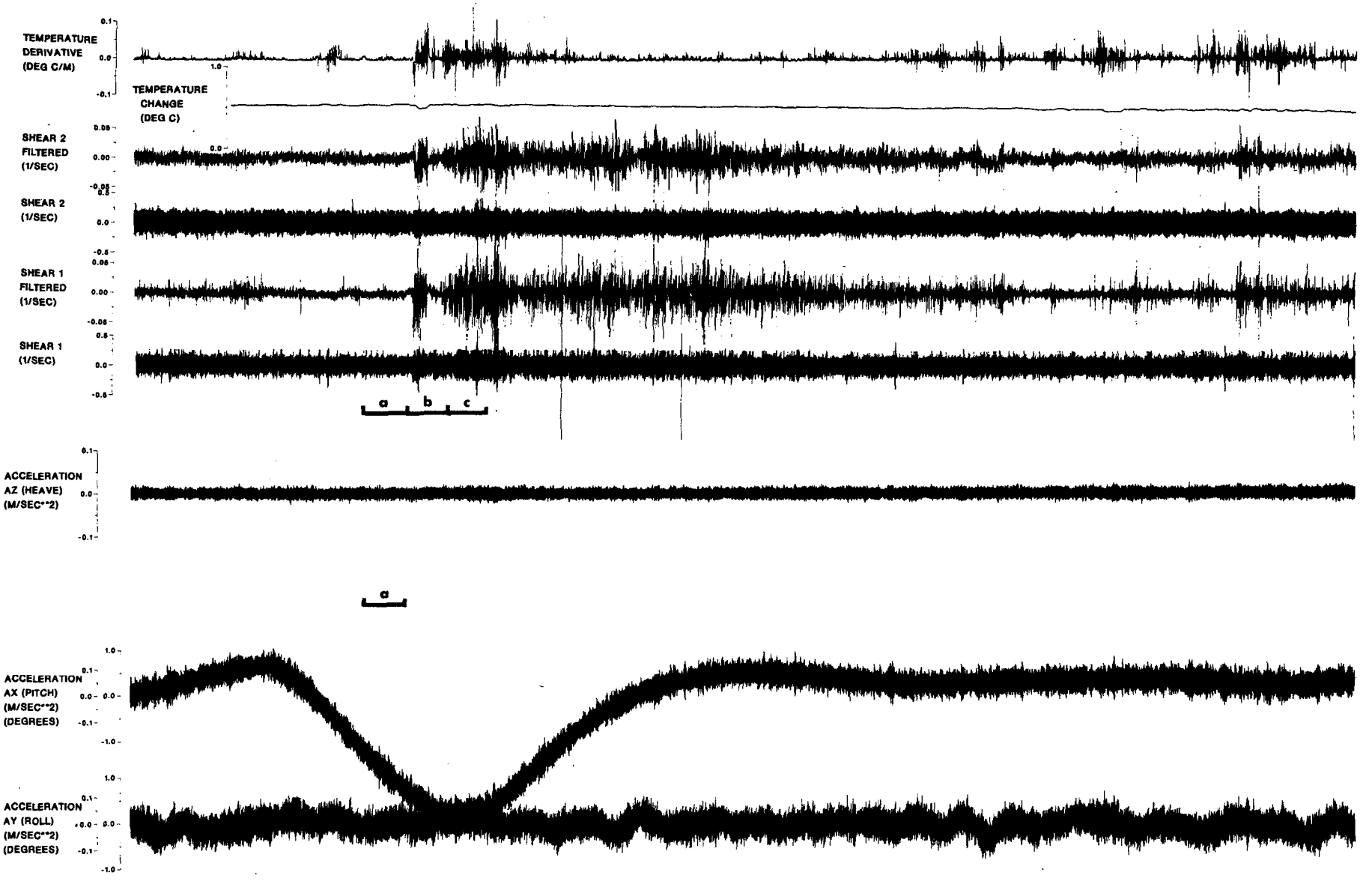

FIG. 9. Turbulent velocity and temperature fluctuations measured at a vessel speed of 1.8 m s^{-1}. The filtered traces have been low-passed at 20 Hz. Shear 1 is $\partial w/\partial x$.

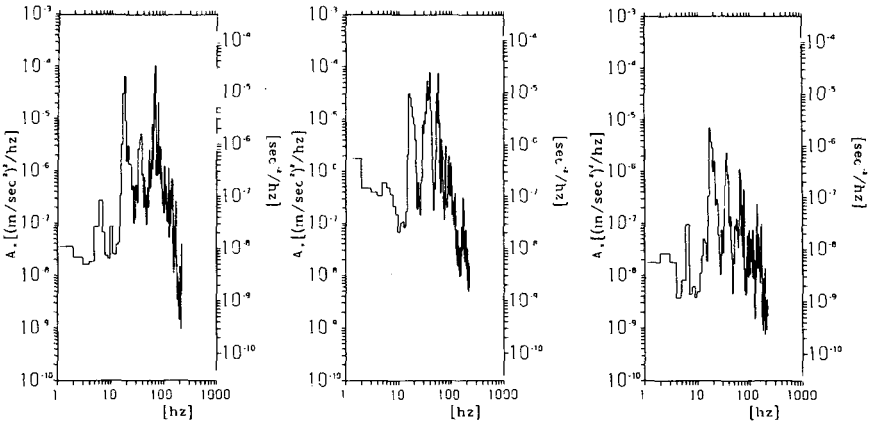

FIG. 10. Spectra of the accelerometer data shown in Fig. 9, corresponding to the block of 4096 points marked by an "a." These spectra can be compared to Fig. 5 to show the increase in vibrational energy with the increase in the speed of the submarine.

the lower wavenumbers, a feature noted by Gargett and Schmitt (1982). There is much more temperature gradient variance in the turbulent patch than in the salt fingers. The peak of the spectrum indicates a cell size of 0.05 m. The real size is uncertain because the orientation of the fingers relative to the line of travel is unknown and we cannot tell if the fingers are cells or sheets. There are no velocity fluctuations detectable in regions A–E. The salinity difference is not large across this region and hence the fingers are not moving fast enough for the velocity signal to be detectable.

In addition to the finger signatures, the region between 35 db and the salinity minimum contains many isolated single- and double-sided spikes in the temperature gradient as well as an enhanced background level of the signal. These features are not believed to be the result of an instrumental problem (as the circuit works well the rest of the time) but, rather, a manifestation of the convection process associated with the ends of the fingers.

The velocity and temperature microstructure data corresponding to the salinity minimum (Fig. 17) reveal two temperature gradient microstructure patches, but only one has associated velocity microstructure. The temperature gradient signals are of different character: the first looks like salt fingers superimposed on a large mean gradient, while the second temperature microstructure patch has widely varying amplitudes that are largest at the upper and lower boundaries. The associated velocity microstructure is forcing the deeper temperature microstructure. The temperature gradient derived from a first difference of the NBIS fast therm-

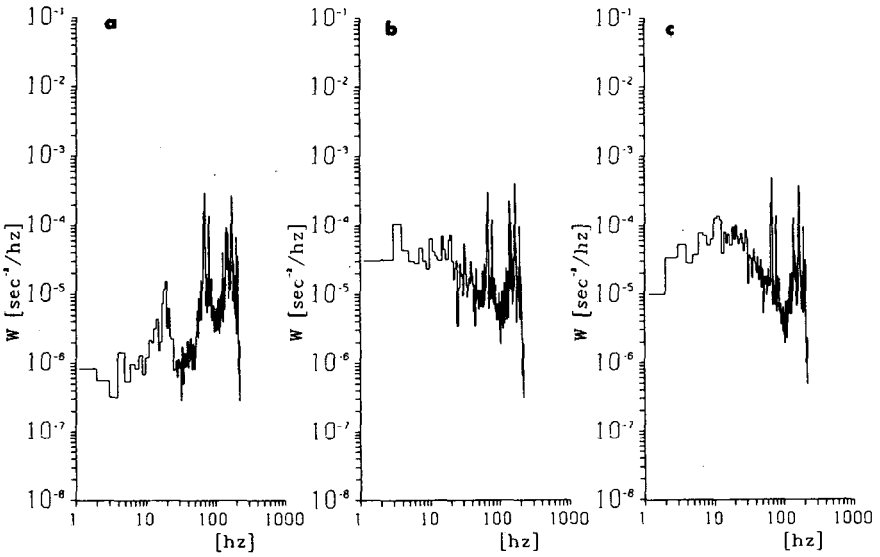

FIG. 11. Spectra of the downstream variation of the vertical-velocity shear, $\partial w/\partial x$, from the data shown in Fig. 9.

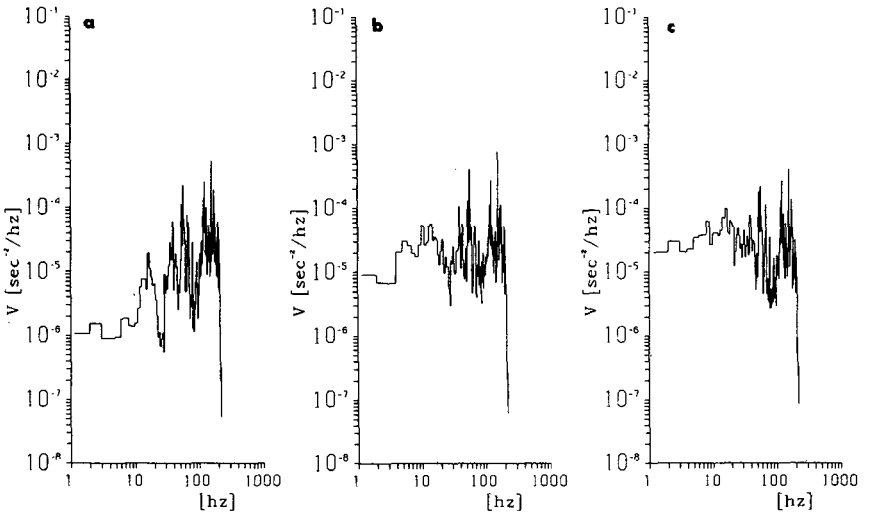

FIG. 12. Spectra of the downstream variation of the lateral horizontal velocity fluctuations, $\partial v/\partial x$. The contamination of the spectra at low signal levels due to the 20 Hz vibration is seen in Fig. 12a.

istor profile (Fig. 18) is very similar to the temperature gradient signal from our turbulence package. The temperature sensors are similar, but the processing is quite different with the NBIS instrumentation digitizing at a much lower frequency (Δt = 0.038 s) making the Nyquist frequency about 13 Hz. With the patches visible in the CTD temperature difference data we can determine the exact position of the patches relative to the salinity minimum without the problems of relating the turbulence sensors to the CTD sensors 0.56 m below. The upper patch is just above the salinity minimum while the lower patch is just below the salinity minimum (Fig. 18).

The T–S plots (Figs. 13 and 18) have constant density lines superimposed on the data. These lines correspond to values of $R\rho = \alpha\Delta T/\beta\Delta S = 1$, lines with twice the slope correspond to $R\rho = 2$ and so forth. Lee (1983) has examined the turbulence and T–S data for this region in detail and concludes that the value of $R\rho$ (deduced from the slope of the T–S curve) is 2–3 in the upper portion of region A, increasing to 3–4 in the middle and increasing to greater than 4 in the lower portion of region A. Regions B and C correspond to an $R\rho$ value of 3. In region D, $R\rho$ varies from 3 to greater than 4. In region E he reports $R\rho > 4$. Finger signatures are found at $R\rho$ values well removed from the fastest growing region between $R\rho = 1$ and 2. The T–S diagram suggests that the bottom of region A has the same water characteristics as regions B and C. If they represent one continuous patch of salt fingering then, the horizontal extent was greater than 230 m. The region with the salt finger signatures seen in Figs. 17 and 18 has an $R\rho$ value of about 2.5 and approaches 2 in places.

There were no salt finger signatures seen in the December 1980 data at the base of the mixed layer. The base of the mixed layer had $R\rho$ between 2 and 3. Linden (1971) showed that the salt finger convection is suppressed when the turbulent velocities become comparable to the fingering velocities. Our noise level for the velocity measurement is apparently greater than the signal level for the fingers off San Diego. The intensity of the fingering process is determined by $R\rho$ and by the magnitude of the temperature and salinity changes across the fingering interfaces. Hence, off San Diego, when the turbulent velocities are above our noise level, they preclude fingers even if the mean profile is favorable.

4. Discussion

There are sufficient data from 4 December 1980 to examine the statistical distribution of ϵ. Monin and Yaglom (1975) report that the lognormal distribution is a good approximation to the integral distribution, but that result does not require that the probability density of the logarithm fit a normal curve well, especially at the tails. Wilson (1977) found the lognormal distribution did not fit especially well except in the case of some crossed-wire data where the sum of the differentiated output from the two channels fitted well even though the individual channels were not lognormally distributed. Stewart *et al.* (1970) looked at atmospheric measurements of velocity fluctuations. Their results show a deficit of large value relative to the lognormal distribution. Marine atmospheric boundary layer measurements by Gibson *et al.* (1970) show no deficit of large values, but their fit only includes the largest 5–30% of their data.

We cannot examine the distribution of the magnitude of the shear as by Stewart *et al.* (1970) or the square of the shear as by Wilson (1977) and Gibson *et*

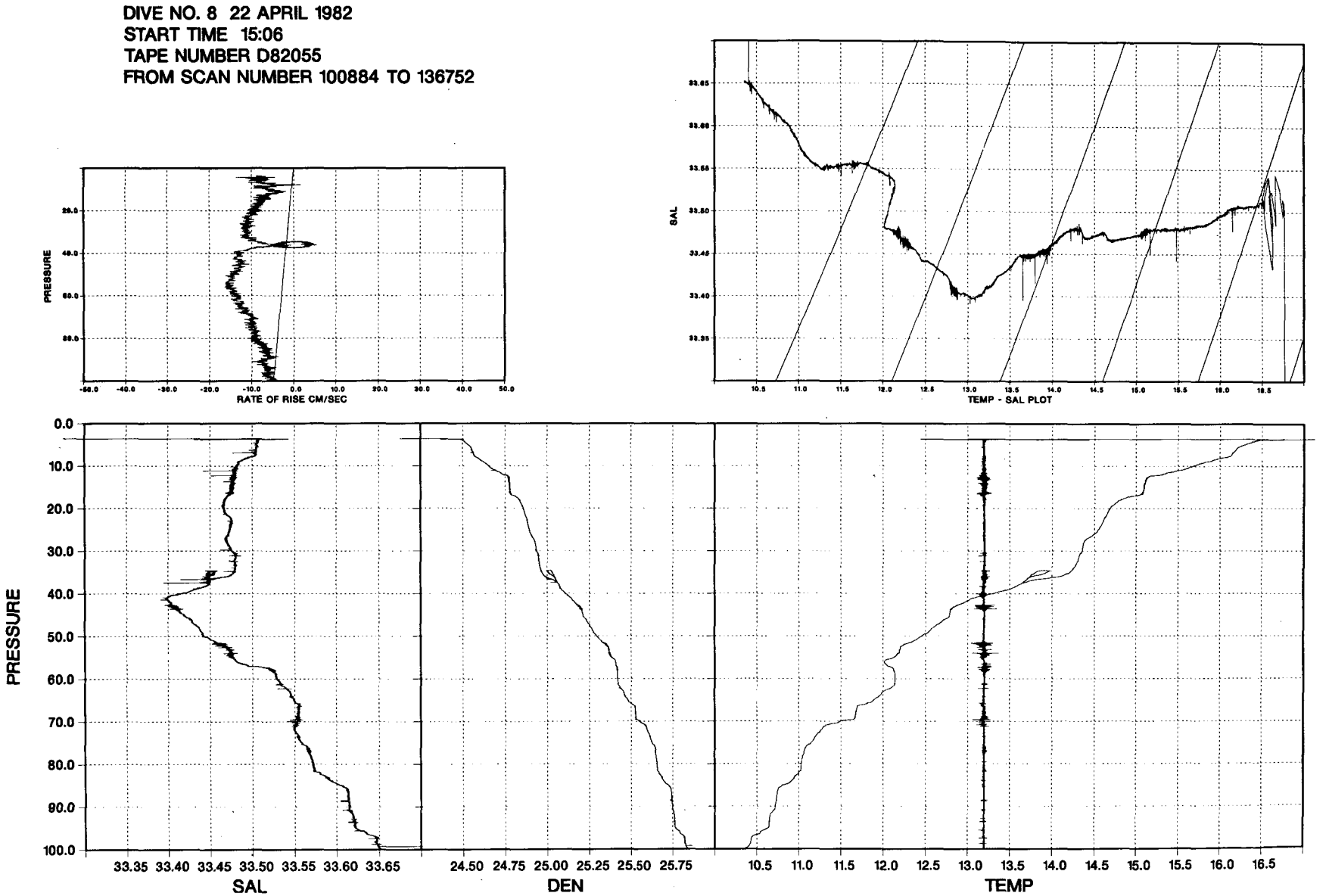

FIG. 13. Temperature, density and salinity traces from 22 April 1982. The temperature–salinity plot has the lines of constant density plotted in addition to the data. The rate of rise is calculated from the pressure data, and is used as an indicator of the vertical speed of the submarine. The ocean surface is located at about 3 db pressure on the plot owing to an offset in the pressure transducer.

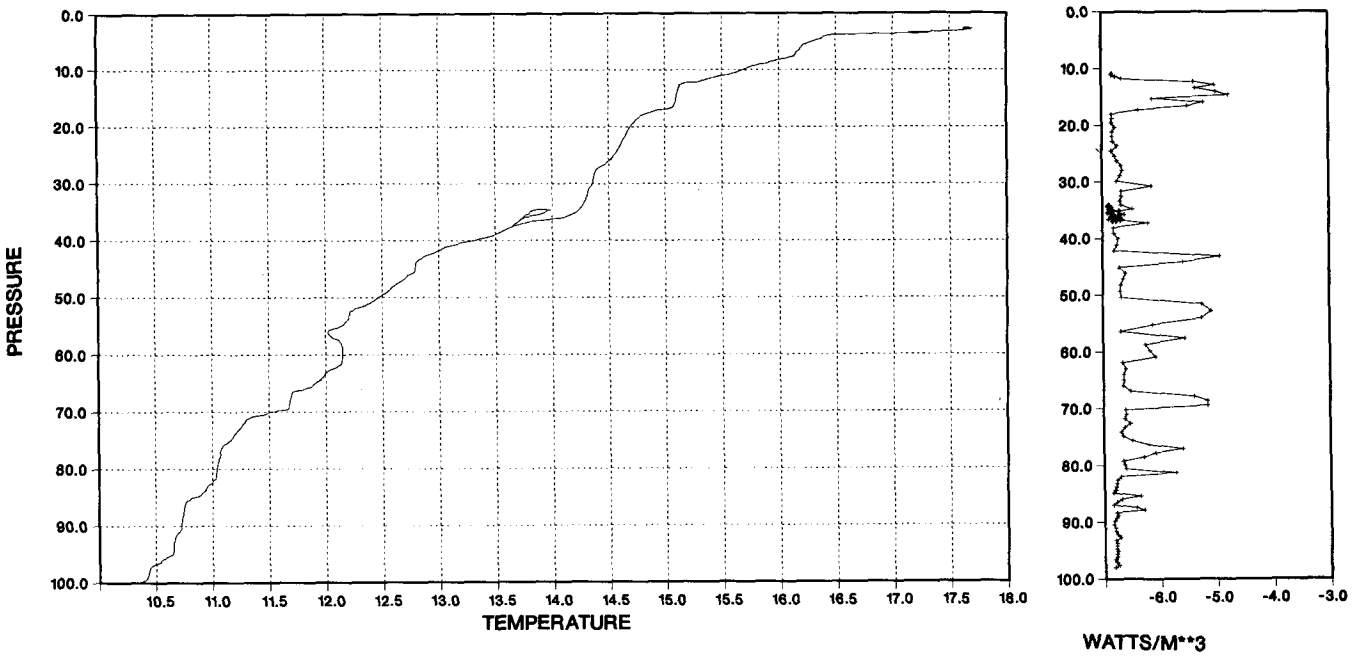

FIG. 14. Dissipation and temperature profiles from 22 April 1982. They have been adjusted for the difference in height between the two sensors.

al. (1970). The vibrational noise must be separated from the signal spectrally and this procedure averages the variance. Averaging a lognormal distribution does not necessarily produce another lognormal distribution. The resulting distribution will approach a normal distribution if the adjacent values are statistically independent (central limit theorem). If the values are highly correlated, then the resulting distribution will still be lognormal. In order to minimize the amount of averaging, ϵ values have been specially recalculated from short data intervals (128 data points corresponding to 0.256 s). Variable integration limits are used as well as the local ship speed. Results from Ninnis (1984) are used to account for the spatial averaging of the probe.

Fitting dissipation values to a lognormal distribution implies that they are all drawn from the same population. A regression analysis of the dissipation estimates above 35 db in Fig. 8 shows a statistically significant (95% confidence level) trend. Dillon and Caldwell (1980) report a similar increase in dissipation with depth, extending to the thermocline during periods of light winds. To minimize contamination of the analysis by the depth dependency, we use only the first part of the data which has a depth range of 4.5 db. (Recall that the submarine started just below 30 db and descended a bit before rising to 15 db.) We do not include the later values when the submarine again passed through this depth range on its way down. There are 2673 individual estimates of ϵ, with all but the lowest few percent above the noise level (Fig. 19). A lognormal distribution fits 80% of the values very well with an excess of small values and a deficit of large values. The comparison is favorable for a larger fraction of the data values than the previously mentioned studies.

The standard deviation for the natural log of the dissipation values is 1.4, so the mean and the median value differ by less than a factor of 3. The mean and standard deviation of the data values are 8.93×10^{-5} and 2.044×10^{-4} W m^{-3}. The mean and standard deviation calculated from the fit line (following Aitchison and Brown, 1963) are 9.59×10^{-5} W and 2.41×10^{-4} W m^{-3}. The lognormal fit overestimates both the mean and standard deviation. Attempts to get a better fit to the distribution by using a Gamma or K distribution, following Jakeman (1980), were unrewarding. The distribution of ϵ estimated from 4224 data points fits the lognormal distribution moderately well. In this case, the standard deviation of the natural logarithm is 0.78. Again, the mean and standard deviation are slightly overestimated because of the deficit of large values. The explanation by Stewart *et al.* (1970) that noise causes the excess of small values is not appropriate for our calculation of ϵ where the effect of noise is to set a lower bound for ϵ and, thus, to lead to a deficit of small values.

The turbulent patch on top of the thermocline (Fig. 8) is similar to active patches in the data from vertical profilers (Osborn, 1978; Gargett *et al.*, 1979). Dissipation measurements indicate that unless the upper layer is strongly forced the turbulence is often more intense in the top of the thermocline than in the mixed layer above it. Dillon and Caldwell (1978) report catastrophic mixing events at the base of the mixed layer,

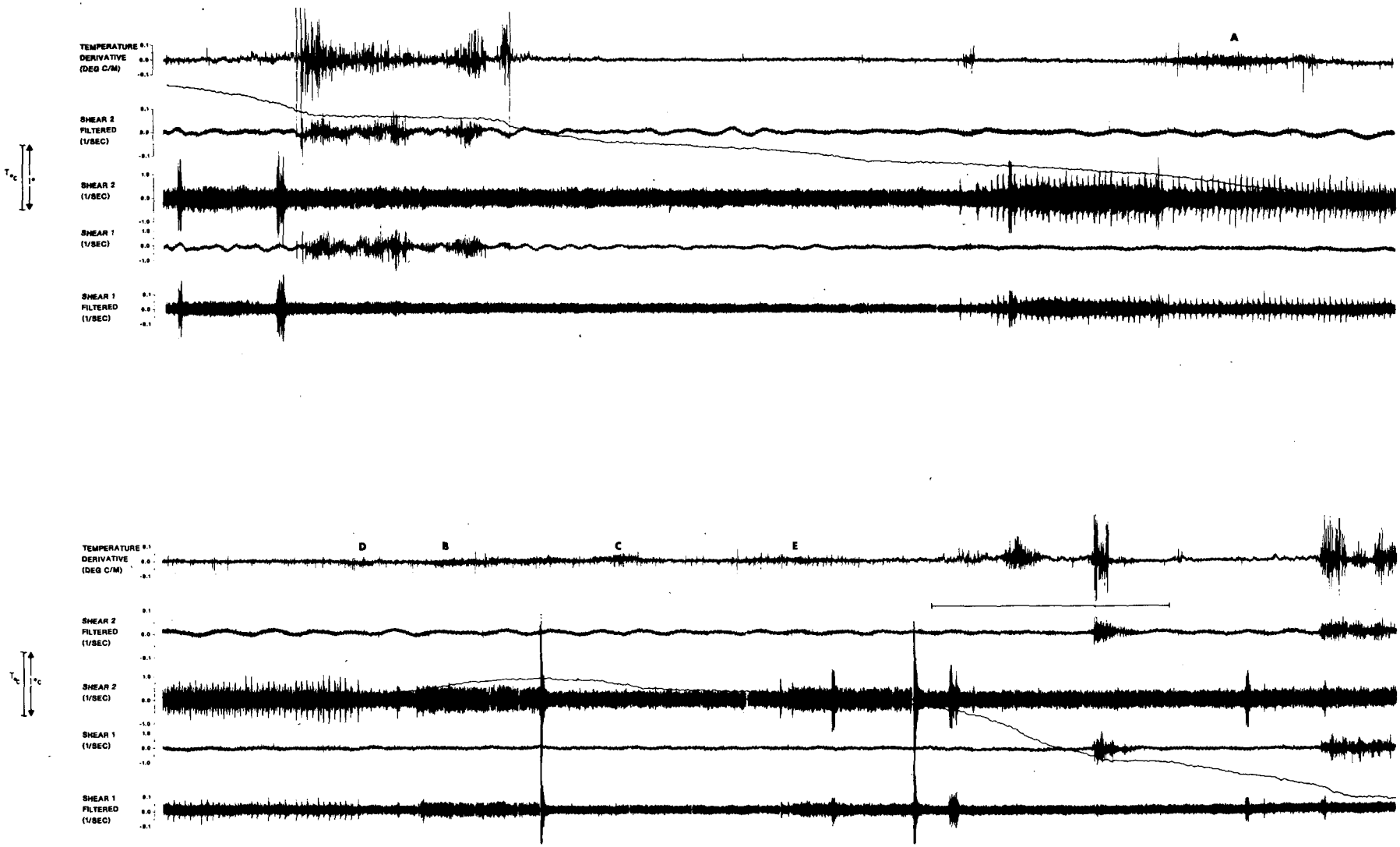

FIG. 15a. Temperature, temperature-gradient and velocity-shear data from 22 April for the interval from 12 to 49 db. The shear data are shown both unfiltered and low-pass filtered at 20 Hz. The lower portion of this figure is marked where it corresponds to Fig. 17. Of interest is the large amount of temperature microstructure (labeled A–E), above the noise level of the system. This region is susceptible to salt fingering. The large regular spikes in part of the unfiltered shear data are from the ballast pump in the submarine. They do not affect the dissipation calculation or appear in the filtered data.

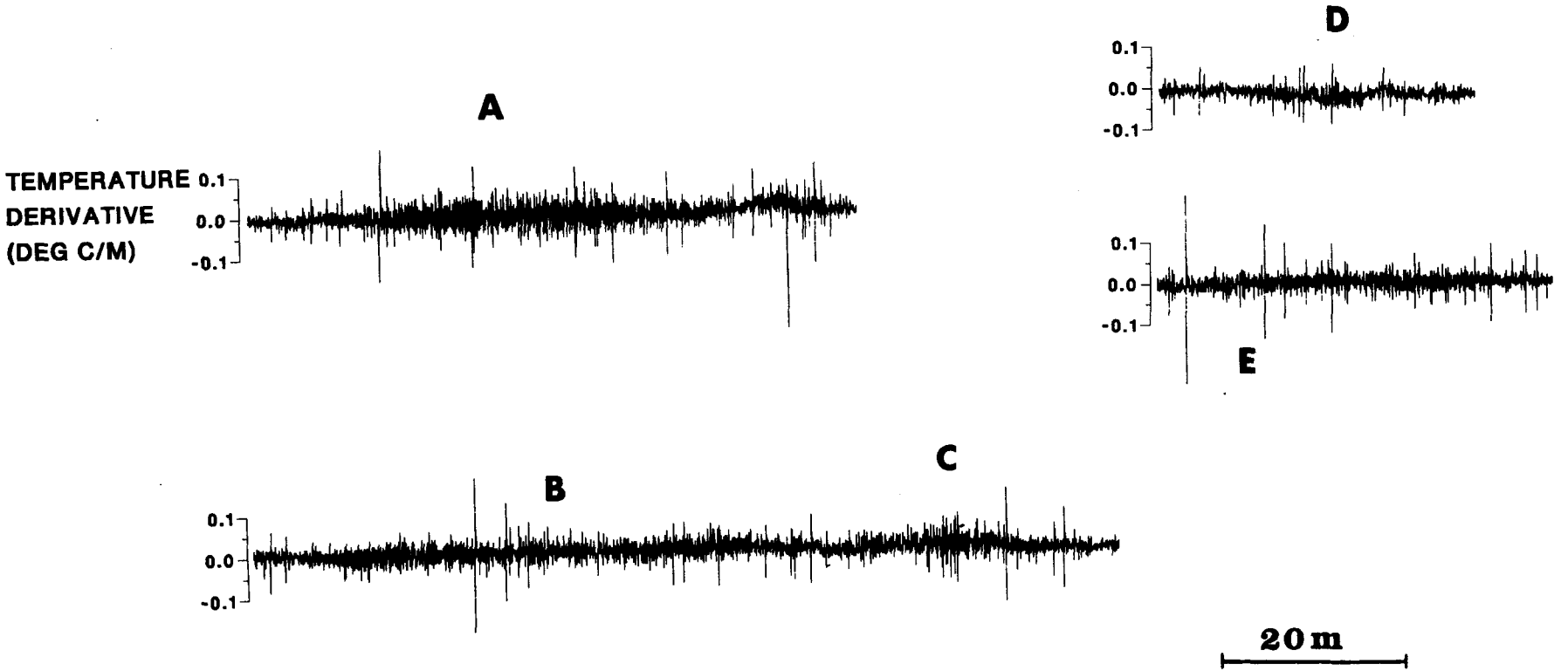

FIG. 15b. Enlarged views of the thermal microstructure seen in the time series shown in Fig. 15a.

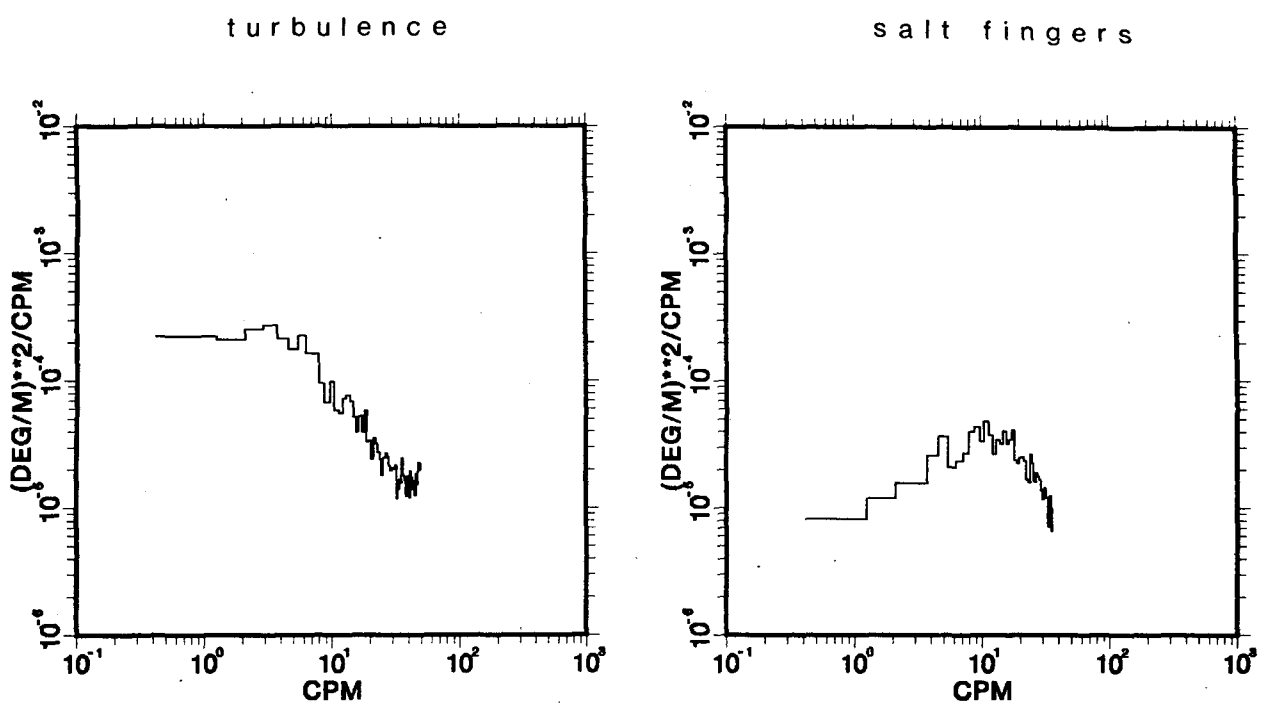

FIG. 16. Spectra of the temperature gradient fluctuations (Fig. 15) show the difference between the salt fingering (region labeled A in Fig. 15), where the signal is band-limited, and the turbulence, where there is substantially more low-wavenumber energy. The turbulent spectrum is from the patch near the start of Fig. 15 and corresponds to the dissipative feature between 10 and 20 db in Fig. 14.

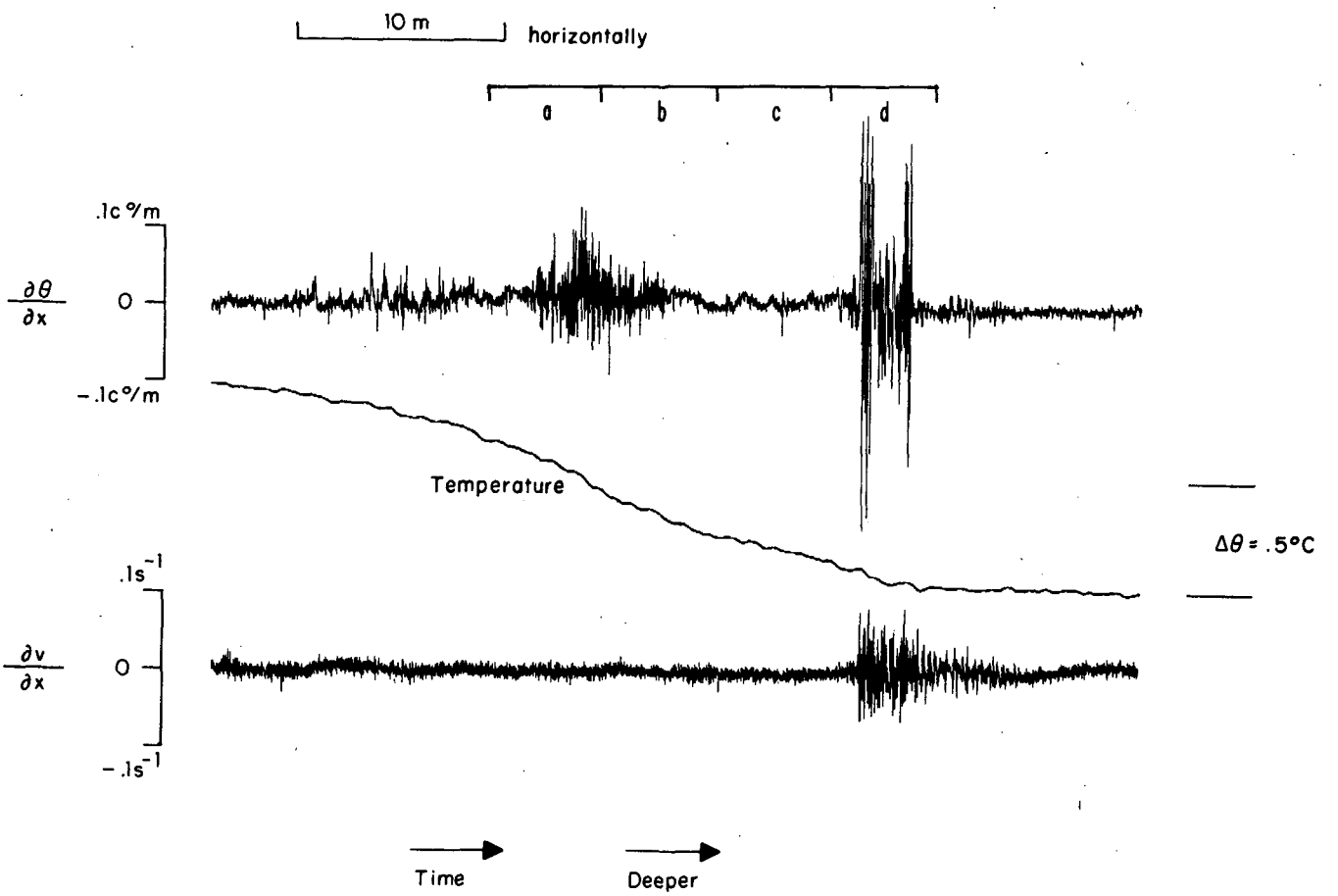

FIG. 17. Temperature, temperature gradient and velocity shear data below 40 db showing two patches of microstructure. The first patch is interpreted as salt fingers, the second as turbulence. These data are marked at the end of Fig. 15.

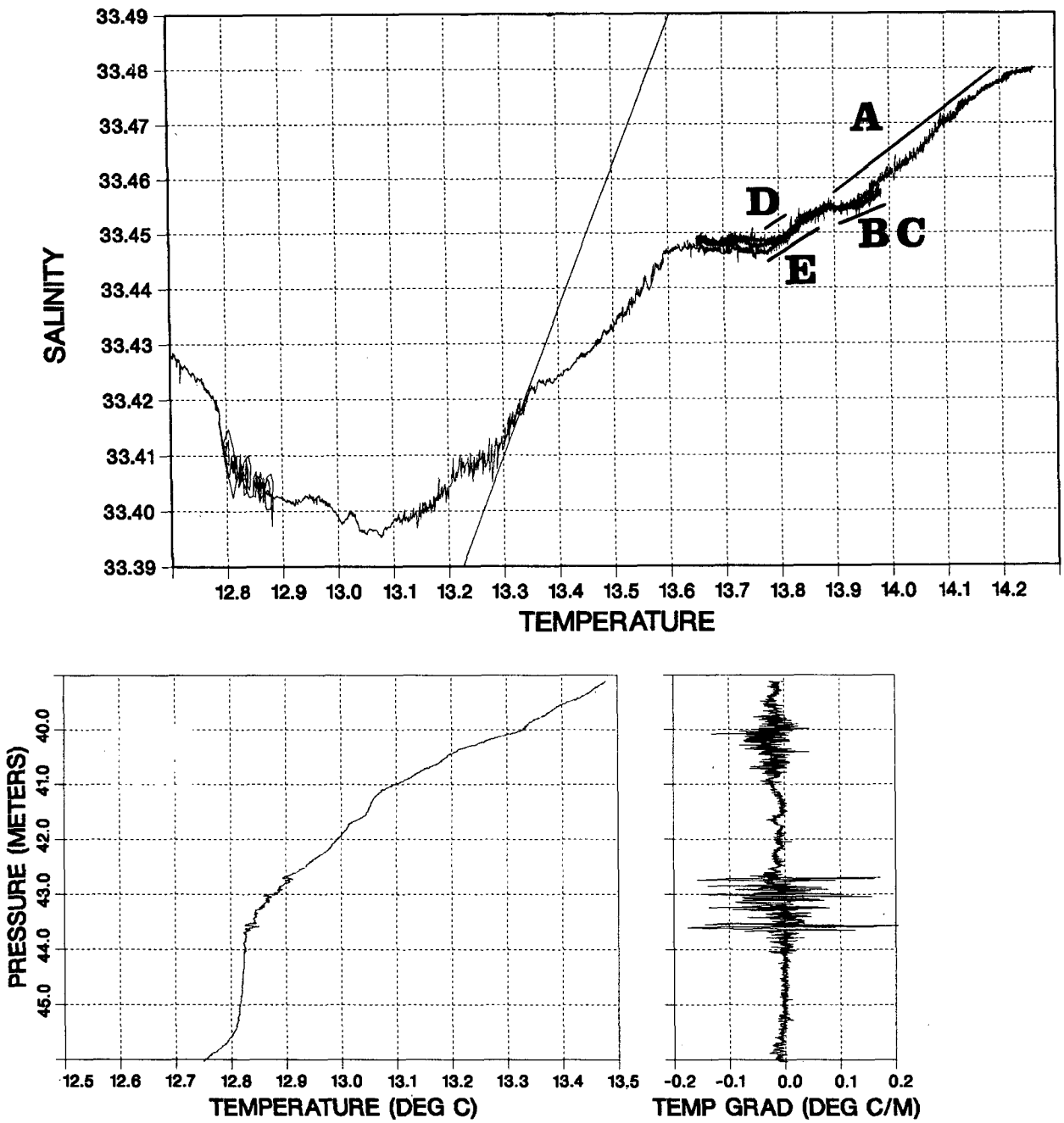

FIG. 18. The profile of temperature data from the fast thermistor on the CTD system and the gradient estimated from its first difference compare favorably to the data from the turbulence package (Fig. 17). The temperature profile is aligned with the temperature-salinity plot for the region of decreasing salinity. Also drawn is a line of constant density. The region of salt fingering, seen in the temperature difference profile, is just above the salinity minimum and the turbulent patch is just below. The regions of regular salt fingering marked in Fig. 15 are identified (following Lee, 1983).

but our temperature profile is similar to their profile of shear generated turbulence. The effect of the stratification on the turbulent velocity shear is apparent spectrally (Fig. 20). The lower wavenumbers are supressed as described by Gargett *et al.* (1984) and reported by Osborn and Lueck (1984) from other *Dolphin* data. The spectra from the well mixed portion of the water column where the ϵ values for the distribution in Fig. 19 were calculated shows no supression of the horizontal velocity shear and a light suppression of the vertical velocity shear. The slope of the low wavenumber end of the spectrum is close to $+1/3$. In the spectrum

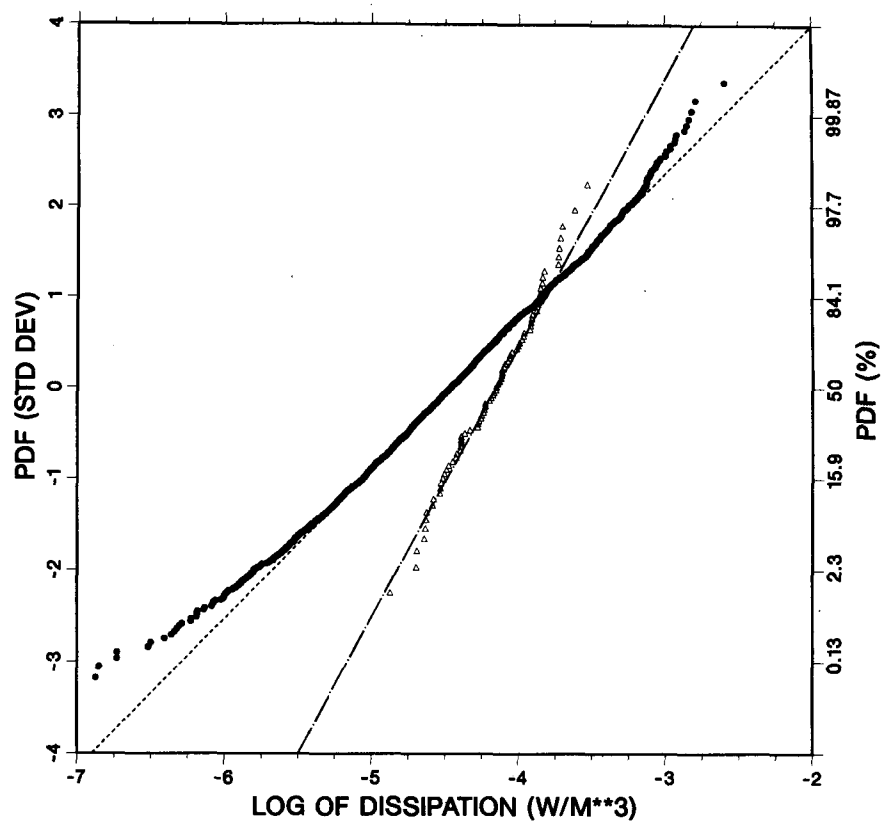

FIG. 19. The probability distribution of the logarithm of the dissipation from 4 December 1980. The solid circles are the estimates from 0.256 seconds of data (128 points) and the open triangles represent averages of 33 adjacent estimates.

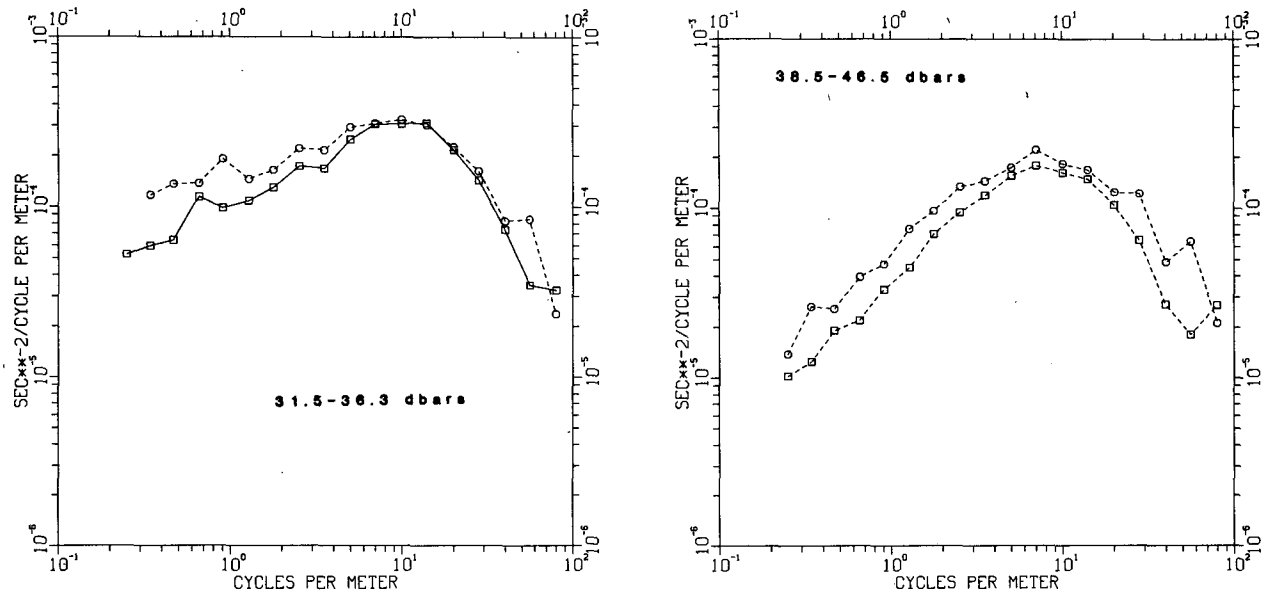

FIG. 20. Spectra of the velocity shear data from a well mixed portion of the upper layer and from the entraining region at the top of the thermocline. These figures were prepared using the procedures described by Osborn and Lueck (1984). The boxes are $\partial w/\partial x$ and the circles are $\partial v/\partial x$.

from the stratified portion of the water column, the low wavenumber ends of the spectra exhibit the +1 slope corresponding to the buoyancy effects reported by Gargett *et al.* (1984).

5. Conclusions

1) The *Dolphin* can measure turbulent dissipation with a noise level of 10^{-7} W m^{-3}.

2) The horizontal temperature gradient measurements show salt fingers with the velocity signals below noise level. Fingers are found at values of $R\rho$ from about 2 to values greater than 4, well above the value for fastest growth. The variance of the temperature gradient is much less in the fingering regimes than in adjacent turbulent patches.

3) The dissipation rates and their distribution in space are similar to those from vertical profilers.

4) Over 80% of the dissipation values from a carefully restricted portion of an active surface mixing layer fit a lognormal distribution. However, we find a deficit of large values and excess of small values, as in atmospheric boundary layers. The standard deviation of the natural logarithm of the dissipation is only 1.4 for 0.3 m spatial averages and 0.78 for 10 m averages.

5) The low wavenumber end of the velocity dissipation spectrum can be strongly diminished by stratification.

Acknowledgments. This work could not have been done without much effort and goodwill on the part of many people. S. Wilson of ONR first suggested the *Dolphin* as a suitable vessel to Ann Gargett. L. Goodman of ONR supported and encouraged the project through many hurdles. The officers and crew of the DOLPHIN were hospitable and helpful. John Benya of NOSC designed, supervised the construction and the installation of the tripod; it is a work of art. Serge Milaire, W. Meyers, Denis Laplante, and Michael Heckl at the University of British Columbia assisted with the instrumentation and data collection. G. Smith, D. Wendstrand, C. Sarrabun, J. Calman and J. Tochko of APL/JHU all supported the work in many ways. The late J. Schedvin of Flow Research helped with preparations and data collection. P. Hendrix performed some of the early CTD calculations. Glen Hunsaker and L. Ford at NOSC assisted with scheduling and arrangements.

This work has been supported by the Office of Naval Research with several contracts over the last five years.

APPENDIX

Errors in ϵ

The technique for estimating dissipation from small-scale velocity measurements using airfoil probes has become popular and accepted over the last 10 years. The probe measures cross-stream velocity fluctuations (Osborn and Crawford 1980); the signal is differentiated to produce a measure of the shear. In this section we assume a familiarity with the probe's operation and discuss the errors in the measurement technique in relation to the submarine operations.

Gargett *et al.* (1984) show that turbulence is isotropic when the buoyancy scale $[l_b = (\epsilon/N^3)^{1/2}]$ is more than 75 times the Kolmogorov scale $(l_k = (\nu^3/\epsilon)^{1/4})$. All the ϵ values in this paper were calculated assuming the isotropic relationship between $\partial w/\partial z$, $\partial v/\partial z$ and ϵ. Often the dissipation is too low in relation to the stratification for the isotropic relation to be strictly valid according to the above criteria.

There are four major sources of uncertainty in the dissipation calculation due to characteristics of the probe:

(i) The probe averages spatially owing to its finite size. The problem is most severe for large ϵ and high temperature where the viscosity is low and the turbulence extends to smaller scales. Ninnis (1984) has measured the spatial response of our probes; the effect is small at low dissipation rates. We incorporated these results in Section 4 where very short intervals were used to calculate the dissipation. Rather than correct the spectra, we used a fit to Ninnis' tabulated results. This approach is suitable for short intervals where the dissipation is relatively uniform but not appropriate for the longer spectra used in the body of the paper. We are presently working on incorporating the spectral correction scheme in our analysis procedure.

(ii) There is an uncertainty in the sensitivity due to uncertainty in the flow speed of the calibrator. This problem is identified separately because the estimated dissipation values are proportional to the fourth power of the flow speed. The nominal error in the flow speed is 1.5%, but sometimes the error has been as large as 6%.

(iii) There are random errors in the calibration procedure, on the order of 4%.

(iv) The probe has a slightly nonlinear response which depends on the angle of attack. If the total angle of attack can be held under 10°, then the sensitivity varies by less than ±5%. This problem arises on the submarine when it changes trim to facilitate diving or when it slews sideways during a turn.

There are three further major sources of uncertainty associated specifically with the submarine measurement:

(v) The mean speed of the submarine is uncertain because of the lack of definitive calibration of the NBIS acoustic current meter. Some simple calibrations have shown the error to be about 5%. This series of calibrations does not include enough information about the sensitivity of the cross-stream components.

(vi) The vibrational contamination of the signal limits the measurement technique at low dissipation levels. Values of ϵ within a factor of 3 of the lowest

values are certainly contaminated by noise. The only way to determine how badly they are contaminated is to reduce the noise level, a difficult procedure. The most reasonable approach is to work in the active regions, to show that the noise level does not matter there, and to use the horizontal platform where its unique capabilities are valuable.

(vii) The flow distortion about the hull and the sensor mount modifies the vorticity field at the sensors. Calculations of the flow distortion due to the potential flow about the hull have been analyzed by Osborn and Lueck (1984). Hunt (1973) shows the fractional change in a component of the vorticity is equal to the fractional change in the length of a parallel-line element. For streamlines at the level of the turbulence sensors:

(a) there is a 5% stretching in the circumference
(b) there is a 3% stretching along streamlines
(c) there is a 5.5% compression between streamlines.

Combining effects (ii)–(v) and assuming statistical independence gives an error of $\pm 26\%$ for ϵ.

REFERENCES

Aitchison, J., and J. A. C. Brown, 1963: *The Log-Normal Distribution.* Cambridge University Press, 176 pp.

Dillon, T. M., and D. R. Caldwell, 1978: Catastrophic events in a surface mixed layer. *Nature,* **276,** 601–602.

——, and ——, 1980: The Batchelor spectrum and dissipation in the upper ocean. *J. Geophys. Res.,* **85,** 1910–1916.

Gargett, A. E., 1975: Horizontal coherence of Oceanic temperature structure. *Deep-Sea Res.,* **22,** 767–776.

——, 1976: An investigation of the occurrence of oceanic turbulence with respect to finestructure. *J. Phys. Oceanogr.,* **6,** 139–156.

——, 1982: Turbulence measurements from a submersible. *Deep-Sea Res.,* **29,** 1141–1158.

——, and R. W. Schmitt, 1982: Observations of salt fingers in the central waters of the eastern North Pacific. *J. Geophys. Res.,* **87,** 8017–8030.

——, T. B. Sanford and T. R. Osborn, 1979: Surface mixing layers in the Sargasso Sea. *J. Phys. Oceanogr.,* **9,** 1090–1111.

——, T. R. Osborn and P. W. Nasmyth, 1984: Local isotropy and the decay of turbulence in a stratified fluid. *J. Fluid Mech.,* **144,** 231–280.

Gibson, C. H., G. R. Stegen and R. B. Williams, 1970: Statistics of the fine structure of turbulent velocity and temperature fields measured at high Reynolds number. *J. Fluid Mech.,* **4,** 153–167.

Grant, H. L., R. W. Stewart and A. Moilliet, 1962: Turbulence spectra from a tidal channel. *J. Fluid Mech.,* **12,** 241–268.

——, A. Moilliet and W. M. Vogel, 1968: Some observations of turbulence in and above the thermocline. *J. Fluid Mech.,* **34,** 443–448.

Gregg, M. C., C. S. Cox and P. W. Hacker, 1973: Vertical microstructure measurements in the central north Pacific. *J. Phys. Oceanogr.,* **3,** 458–469.

Hunt, J. C. R., 1973: A theory of turbulent flow round two-dimensional bluff bodies. *J. Fluid Mech.,* **61,** 625–706.

Jakeman, E., 1980: On the statistics of *K*-distributed noise. *J. Phys. A: Math. Nucl. Gen.,* **13,** 31–48.

Lee, S. I., 1983: Density structure associated with salt fingers. M.S. thesis, U.S. Naval Postgraduate School, 48 pp.

Linden, P. F., 1971: Salt finger in the presence of grid-generated turbulence. *J. Fluid Mech.,* **49,** 611–624.

Miyake, Y., and M. Koizumi, 1948: The measurement of the viscosity coefficient of seawater. *J. Mar. Res.,* **7,** 63–66.

Monin, A. S., and A. M. Yaglom, 1975: *Statistical Fluid Mechanics,* Vol. 2. MIT Press, 873 pp.

Moum, J. N., and R. G. Lueck, 1985: Causes and implications of noise in oceanic dissipation measurements. *Deep-Sea Res.,* (in press).

Nasmyth, P. W., 1970: Oceanic turbulence. Ph.D. thesis, University of British Colombia, 69 pp.

Ninnis, R., 1984: The spatial transfer function of the airfoil turbulence probe. Ph.D. thesis, University of British Colombia, 94 pp.

Osborn, T. R., 1974: Vertical profiling of velocity microstructure. *J. Phys. Oceanogr.,* **4,** 109–115.

——, 1978: Measurements of energy dissipation adjacent to an island. *J. Geophys. Res.,* **83,** 2939–2957.

——, and C. S. Cox, 1972: Oceanic fine-structure. *Geophys. Fluid Dyn.,* **3,** 321–345.

——, and W. R. Crawford, 1980: An airfoil probe for measuring turbulent velocity fluctuations in water. *Air–Sea Interaction,* F. Dobson, L. Hasse and R. Davis, Eds., Plenum, 801 pp.

——, and R. G. Lueck, 1984: Oceanic shear spectra from a submarine. *Proc. 'Aha Huliko'a Hawaiian Winter Workshop,* Honolulu, U.S. Office of Naval Research, Hawaiian Institute of Geophysics, and Dept. of Oceanogr. University of Hawaii, 25–50.

——, and ——, 1985a: *Dolphin* instrumentation and operations. Manuscript Rep., Naval Postgraduate School.

——, and ——, 1985b: Turbulence measurements with a towed body. *J. Atmos. Ocean. Technol.,* (in press).

——, —— and A. E. Gargett, 1981: *Dolphin* data. Department of Oceanography, University of British Columbia, Manuscript Rep. No. 36, 34 pp.

Stewart, R. W., R. Wilson and R. W. Burling, 1970: Some statistical properties of small scale turbulence in atmospheric boundary layer. *J. Fluid Mech.,* **41,** 141–152.

Turner, J. S., 1973: *Buoyancy Effects in Fluids.* Cambridge University Press, 367 pp.

Wilson, J. R., 1977: Some observed statistical properties of small scale turbulence. Ph.D. thesis, University of British Colombia, 125 pp.